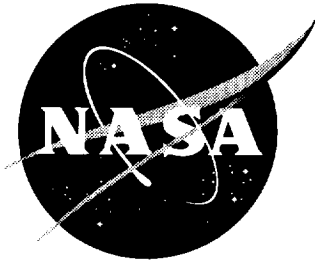


NASA/TM-1999-209689



# Temperature Control of Avalanche Photodiode Using Thermoelectric Cooler

*Tamer F. Refaat  
Old Dominion University, Norfolk, Virginia*

*William S. Luck, Jr. and Russell J. DeYoung  
Langley Research Center, Hampton, Virginia*

National Aeronautics and  
Space Administration

Langley Research Center  
Hampton, Virginia 23681-2199

---

October 1999

---

Available from:

NASA Center for AeroSpace Information (CASI)  
7121 Standard Drive  
Hanover, MD 21076-1320  
(301) 621-0390

National Technical Information Service (NTIS)  
5285 Port Royal Road  
Springfield, VA 22161-2171  
(703) 605-6000

## 1. Introduction

The avalanche photodiode (APD) is a solid state, quantum, optical detector which uses the photo-generation of charge carriers in order to detect light. APDs are highly recommended for low-light optical detection applications in the visible and near infrared region due to their linearity with incident light intensity, compactness, ruggedness, and relatively large internal gain. The APD output current is dependent on both the operating temperature and the bias voltage of the device (ref. 1 and 2). The bias voltage can be set using a stable, high-voltage source. To address the temperature dependence of the output current, many APD packages come with a built-in thermoelectric cooler (TEC) for accurately controlling the operating temperature (ref. 3).

This memorandum reviews the theory of thermoelectric cooling. Also, the design and performance of a proportional integral (PI) temperature controller and its application to an EG&G APD package (C30649E), which includes a built-in TEC and a thermistor, are discussed. This APD package was chosen, after characterizing a group of APDs, in order to develop an advanced detection system for atmospheric water vapor DIAL measurements (ref. 2, 4, 5 and 6).

## 2. APD Temperature Dependence

An APD is a device similar to a rectifier diode, except its output current contains a term which is dependent on the incident light intensity on its surface in the operating wavelength range. The APD output current is given by (ref. 1, 7 and 8)

$$I_{APD} = -I_d + I_s \left( e^{\frac{qV}{kT}} - 1 \right) \quad (1)$$

where  $I_{APD}$  is the APD output current,  $I_d$  is the detected photo-current,  $I_s$  is the saturation dark current,  $q$  is the electron charge,  $V$  is the device bias voltage (negative for reverse bias),  $k$  is Boltzmann's constant, and  $T$  is the temperature. The second term of equation (1) represents the APD dark current and the first term,  $I_d$ , represents the photo-current, given by (ref. 1, 7 and 8)

$$I_d = \mathfrak{R} \cdot P \quad (2)$$

where  $\mathfrak{R}$  is the APD responsivity, and  $P$  is the incident optical power. The APD responsivity,  $\mathfrak{R}$  (A/W), is obtained from (ref. 1, 7 and 8)

$$\mathfrak{R} = \eta G \cdot \frac{q}{hc} \cdot \lambda \quad (3)$$

where  $\eta$  is the wavelength dependent quantum efficiency,  $G$  is the APD internal gain,  $h$  is Planck's constant,  $c$  is the speed of light, and  $\lambda$  is the wavelength of the incident light. At a constant bias voltage, the APD operating temperature affects its output current. The APD gain, and therefore its responsivity, is a strong function of the device temperature. On the other hand, the APD dark current, as well as the dark current noise, is also dependent on the APD temperature.

At a constant bias voltage and wavelength, the APD responsivity increases by decreasing the device temperature. Therefore, cooling the APD is recommended to increase its detected photo-current. Figure 1 clearly indicates this fact by showing the responsivity-versus-temperature relations at three different wavelengths for a 336V bias voltage (ref. 2, 7 and 8).

The APD dark current, given by the second term of equation (1), is also dependent on the device operating temperature. Decreasing the APD temperature will increase the dark current. The maximum dark current will be obtained at a temperature of 0 K and will be equal to the saturation current.

More importantly, the APD dark current is associated with noise, known as the dark current shot noise, which is given by (ref. 9 and 10)

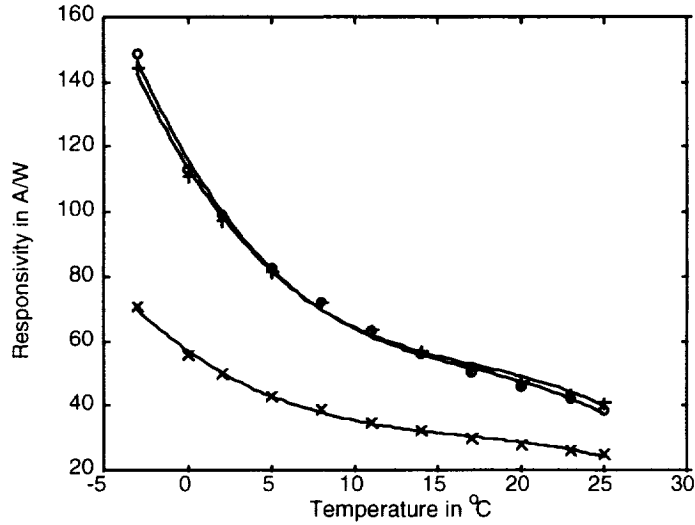


Figure 1. EG&G C30649E responsivity variation with temperature at 336 V bias at (o) 720 nm, (+) 820 nm and (x) 940 nm. (See ref. 2)

$$i_n^2 = 2qGFB \left[ I_s \left( e^{\frac{qV}{kT}} + 1 \right) + I_d \right] \quad (4)$$

where  $i_n$  is the shot noise current,  $F$  is the excess noise factor, and  $B$  is the device bandwidth. The APD temperature affects the dark current shot noise directly in the denominator of the exponential power and indirectly by its effect on the device gain. The first effect is dominant; and for a reverse bias voltage, the dark current shot noise is reduced by reducing the operating temperature.

In most applications, the effect of the APD dark current on the output signal can be eliminated by either modulating the input optical signal (ref. 2) or by subtracting the dark current from the device output (ref. 4). Therefore, low temperature operation of APDs is recommended in order to increase the device responsivity and to reduce the dark current shot noise.

### 3. Thermoelectric Coolers

A thermoelectric cooler module consists of an array of semiconductor (group V-VI, e.g. bismuth telluride) pellets that have been positively (p) or negatively (n) doped. The p-n pellet pairs are connected electrically in series and thermally in parallel (ref. 11, 12 and 13). Consider a simple thermoelectric cooling unit, as illustrated in figure 2, in which the electrical resistance between the semiconductor elements and metal links, as well as the resistances of the links themselves, are negligible. Also, the thermal resistance between the semiconductor pair, the heat source, and the heat sink are neglected. For simplicity, all of the material thermal coefficients are assumed constant and independent of temperature.

#### 3.1. TEC Theory of Operation

TEC operation is based on the Peltier effect which results in the transport of heat when electric current flows in a conductor (ref. 11 and 13). This heat flow is revealed only at a junction between two different materials where the heat transport on either side is different. In the two branches of figure 2, the heat transported (Watts) from the source is given by (ref. 11)

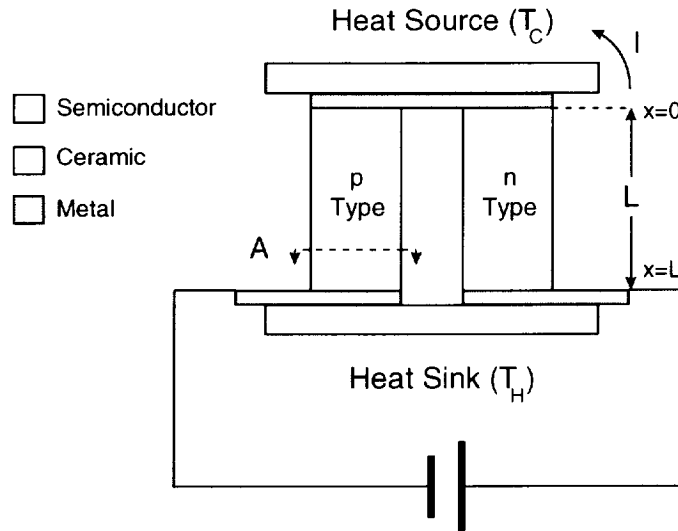


Figure 2. A TEC p-n pair.

$$q_p = \alpha_p IT - \kappa_p A \frac{dT}{dx} \quad (5)$$

$$q_n = -\alpha_n IT - \kappa_n A \frac{dT}{dx} \quad (6)$$

where  $\alpha_p$  and  $\alpha_n$  are the Seebeck coefficients ( $WK^{-1}A^{-1}$ ) of the p and n materials, respectively,  $\kappa_p$  and  $\kappa_n$  are their thermal conductivity ( $Wm^{-1}K^{-1}$ ),  $I$  is the TEC current,  $A$  is the semiconductor pellet cross-sectional area, and  $T$  is the temperature.  $\alpha_n$  is a negative quantity, and the thermoelectric heat flow from the source through both branches is positive and is opposed by the effect of thermal conduction. Within

the branches, the rate of generation of heat per unit length ( $\text{Js}^{-1}\text{m}^{-1}$ ) from the Joule effect is given by (ref. 11)

$$-\kappa_p A \frac{d^2 T}{dx^2} = \frac{I^2 \rho_p}{A} \quad (7)$$

$$-\kappa_n A \frac{d^2 T}{dx^2} = \frac{I^2 \rho_n}{A} \quad (8)$$

where  $\rho_p$  and  $\rho_n$  are the electrical conductivity ( $\Omega\text{m}$ ) of the p and n materials, respectively. Now, if the branches are of length  $L$ , then the boundary conditions are  $T=T_C$  at  $x=0$ , and  $T=T_H$  at  $x=L$ . Solving differential equations (7) and (8) and substituting in differential equations (5) and (6) at  $x=0$ , we get (ref. 11)

$$q_p = \alpha_p I T_C - \frac{\kappa_p A (T_H - T_C)}{L} - \frac{I^2 \rho_p L}{2A} \quad (9)$$

$$q_n = -\alpha_n I T_C - \frac{\kappa_n A (T_H - T_C)}{L} - \frac{I^2 \rho_n L}{2A} \quad (10)$$

The cooling power  $Q_C$  at the sink is the sum of the above two equations and is given by

$$Q_C = \alpha I T_C - K (T_H - T_C) - \frac{1}{2} I^2 R \quad (11)$$

where  $\alpha = \alpha_p - \alpha_n$  is the differential Seebeck coefficient of the unit. The thermal conductance,  $K$ , of the two branches in parallel is given by

$$K = \frac{\kappa_p A}{L} + \frac{\kappa_n A}{L} \quad (12)$$

and the electrical resistance  $R$  of the two branches in series is given by

$$R = \frac{\rho_p L}{A} + \frac{\rho_n L}{A} \quad (13)$$

From equation (11), it is interesting to note that the reversible cooling process (represented by the first term) is opposed by the sum of two irreversible processes, which are the heat conduction (represented by the second term) and half the joule heating (represented by the power loss in the third term).

The electrical power consumed in the branches is given by (ref. 11)

$$P_p = \alpha_p I (T_H - T_C) + \frac{I^2 \rho_p L}{A} \quad (14)$$

$$p_n = -\alpha_n I(T_H - T_C) + \frac{I^2 \rho_n L}{A} \quad (15)$$

Thus, the total power input is given by the sum of equations(14) and (15)

$$P = \alpha I(T_H - T_C) + I^2 R \quad (16)$$

Applying the first law of thermodynamics, the heating power,  $Q_H$ , at the sink is the sum of equations (11) and (16) and is given by

$$Q_H = \alpha I T_H - K(T_H - T_C) + \frac{1}{2} I^2 R \quad (17)$$

Finally, the system efficiency is examined by the coefficient of performance,  $\phi$ , which is the ratio of the rate at which heat is extracted from the source to the rate of expenditure of electrical energy (ref. 11 and 13). Using equations (11) and (16), the coefficient of performance is given by

$$\phi = \frac{Q_C}{P} = \frac{\alpha I T_C - K(T_H - T_C) - \frac{1}{2} I^2 R}{\alpha I(T_H - T_C) + I^2 R} \quad (18)$$

For a certain temperature difference, the current,  $I_m$ , for maximum coefficient of performance,  $\phi_m$ , can be evaluated by setting  $d\phi/dI = 0$ . In this case,  $\phi_m$  is given by

$$\phi_m = \frac{T_C \left[ (1 + Z T_m)^{1/2} - (T_H / T_C) \right]}{(T_H - T_C) \left[ (1 + Z T_m)^{1/2} + 1 \right]} \quad (19)$$

where  $Z$  is the TEC figure of merit, which is given by (ref. 11 and 13)

$$Z = \frac{\alpha^2}{KR} \quad (20)$$

and  $T_m$  is the average temperature which is given by

$$T_m = \frac{T_H + T_C}{2} \quad (21)$$

### 3.2. TEC Cooling Cycle

The TEC cooling cycle can be further understood in a qualitative manner by studying the energy band diagram of its materials, as shown in figure 3. An electron at the cold metal absorbs a heat quanta, which leads to an increase in the electron's potential energy. The applied electric field from the supply causes the electron to drift to the n-material. A fraction of the electron energy is converted to kinetic energy as

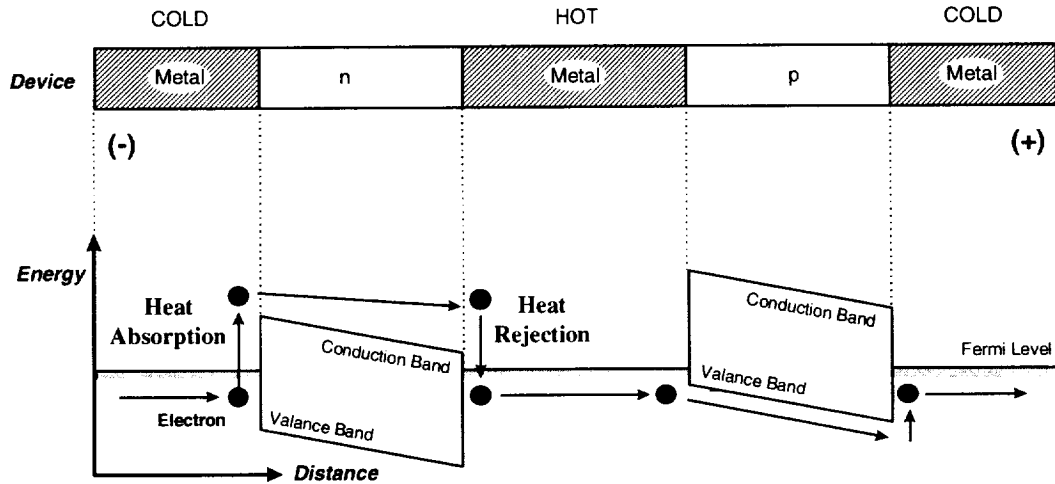


Figure 3. Energy band diagram for a thermoelectric cooling unit.

the electron proceeds through the n-material. At the end of the n-material, the electron rejects its energy gain to the hot metal in the form of heat. In order to complete the cycle, the electron must reject more energy to pass through the p-material using the lower band. On the other hand, at the p-material cold-metal junction, the electron gains more energy, through heat absorption, in order to complete its cycle.

Similarly, the holes do the same thing in the opposite direction, which leads to a heat transfer from the cold metal to the hot metal by both charge carriers. The power supply must provide the energy for the carriers to continue the cycle and also provide the system with the energy that is lost due to the electrical resistance of the cooling unit.

#### 4. APD Temperature Controller

The EG&G APD C30649E package, shown schematically in figure 4, is supplied with a built-in TEC cooler to control the detector temperature. The temperature status of the APD is sensed by the thermistor, which is located as close as possible to the APD in order to ensure a minimal temperature gradient between the two devices. For this particular thermistor, the relation between its resistance ( $\Omega$ ) and the temperature (K) is given by (ref. 3)

$$R_T = 10^4 \cdot \exp \left[ 3940 \left( \frac{1}{T} - \frac{1}{298} \right) \right] \quad (22)$$

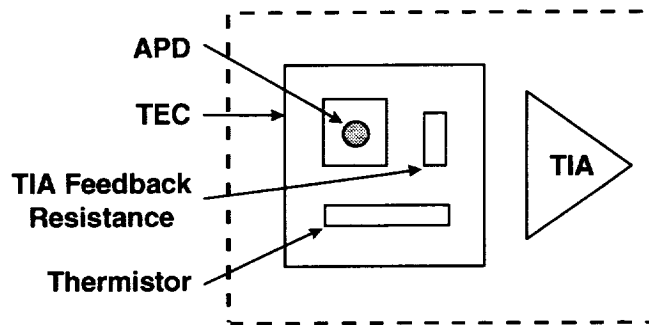


Figure 4. APD package physical diagram.

The APD temperature controller circuit is shown in the circuit diagram of figure 5. The APD temperature feedback is obtained by placing the thermistor in an arm of a Wheatstone bridge. The remaining arms are formed by three equal-valued resistors,  $R_S$ . According to equation (22), the value of  $R_S$  determines the balance condition of the bridge and sets the detector temperature to a value given by

$$T = \left\{ \frac{\ln\left(\frac{R_S}{10^4}\right)}{3940} + \frac{1}{298} \right\}^{-1} \quad (23)$$

The bridge is supplied by the zener diode,  $D$ , with a zener voltage  $V_Z$ .  $R_Z$  is a current-limiting resistor which stabilizes the zener diode voltage and prevents its break down.

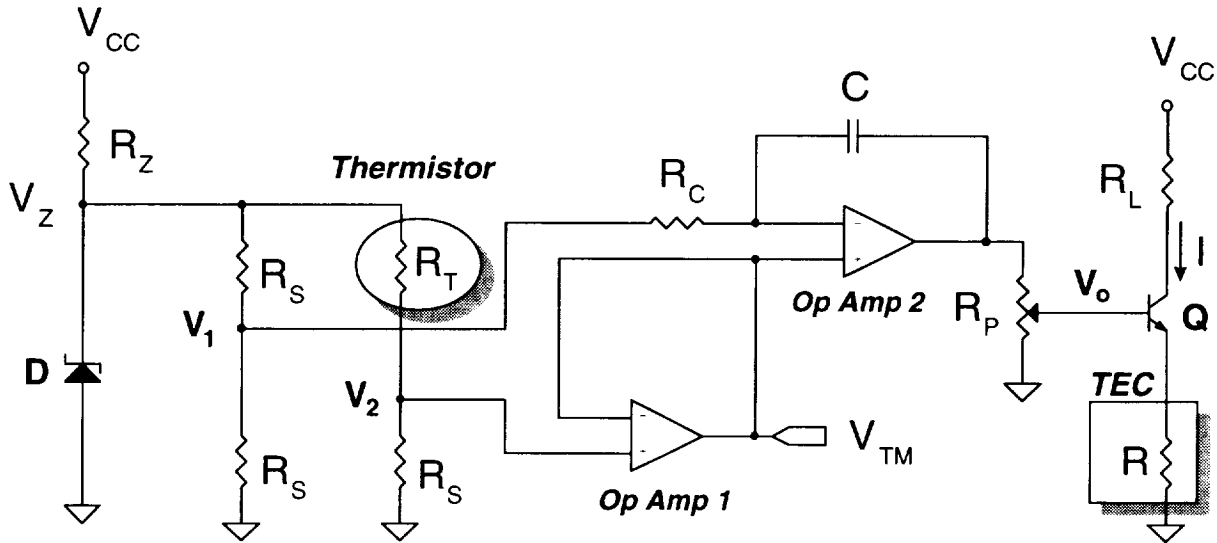


Figure 5. APD temperature controller circuit diagram.

The bridge balance error,  $V_2 - V_1$ , is sensed by a PI controller formed by two operational amplifiers (op amp's). Op amp 1 acts as a voltage follower with an output voltage  $V_{TM}$ . This voltage is used to monitor the APD operating temperature. The output of op amp 2 is applied to a potentiometer,  $R_P$ , to set the TEC current by controlling the emitter current of transistor  $Q$ . The setting of  $R_P$  changes the controller overall gain  $K_{PI}$ . According to the analysis of the circuit shown in figure 5, the controller input-output relation is given by

$$V_o = K_{PI} \left[ V_2 + \frac{1}{sCR_C} (V_2 - V_1) \right] \quad (24)$$

In terms of the error signal,  $E_{rr}$ , defined as the difference between  $V_2$  and  $V_1$ , the same equation can be rewritten as

$$V_o - K_{PI}V_1 = K_{PI} \left[ 1 + \frac{1}{sCR_C} \right] E_{rr} \quad (25)$$

Resistor  $R_L$  is used to limit the TEC current that corresponds to its maximum value (See Appendix A). The temperature monitor voltage reading,  $V_{TM}$ , is given in terms of the zener voltage as

$$V_{TM} = \frac{R_S}{R_S + R_T} V_Z \quad (26)$$

If the APD temperature reaches its steady state value, the monitor voltage is given by

$$V_{TM} = \frac{1}{2} V_Z \quad (27)$$

Appendix B gives the value of the controller circuit components used to construct this controller.

## 5. Heat Load Estimation

The heat loads at the cold side of the TEC cooler are due to active and passive heat sources. In the EG&G C30649E APD package, the detector output photo-current variation is converted into a voltage variation by a trans-impedance amplifier (TIA) (ref. 1, 2 and 3). The feedback resistor  $R_F$  of this amplifier is cooled by the same TEC cooler in order to reduce the Johnson noise. The APD, thermistor, and TIA feedback resistor define the three active heat loads  $Q_{APD}$ ,  $Q_{THR}$ , and  $Q_{TIA}$ , respectively. The power consumed in these elements is directly transformed to heat and is given, respectively, by.

$$Q_{APD} = V_{BIAS} \cdot I_{APD} \quad (28)$$

$$Q_{THR} = \frac{R_T}{(R_T + R_S)^2} V_Z^2 \quad (29)$$

$$Q_{TIA} = I_{APD}^2 \cdot R_F \quad (30)$$

TEC passive heat loads come from the temperature gradient between the cooled components and the ambient environment. The first passive load,  $Q_{RAD}$ , is the heat radiation from the ambient environment to the TEC cold side and is given by (ref. 12)

$$Q_{RAD} = F \cdot e \cdot s \cdot A_{TEC} (T_{amb}^4 - T_C^4) \quad (31)$$

where  $F$  is the surface shape factor,  $e$  is the surface emissivity,  $s$  is the Stefan-Boltzmann constant,  $A_{TEC}$  is the area of the TEC cold surface, and  $T_{amb}$  is the ambient temperature. The second passive load,  $Q_{CON}$ ,

is due to the conduction between the TEC cold surface and the ambient environment through the air space below the package window, which has a length  $L_P$  (see Appendix A). This is given by (ref. 12)

$$Q_{CON} = \frac{K_{Air} A_{TEC}}{L_P} (T_{amb} - T_C) \quad (32)$$

where  $K_{air}$  is the air thermal conductivity.

At the TEC hot side, heat accumulation will lead to device failure. Therefore, a heat sink is used for heat dissipation to the ambient environment. Considering the worst-case situation in which the heat transfer from the heat sink to the ambient environment is only through radiation, the amount of heat radiated from the heat sink,  $Q_{HS}$ , is given by

$$Q_{HS} = F \cdot e \cdot s \cdot A_{HS} (T_H^4 - T_{amb}^4) \quad (33)$$

where  $A_{HS}$  is the heat sink surface area.

The heat transfer problem is summarized in the power flow diagram of figure 6. Assuming the worst case in which the surface shape factor and emissivity are both equal to one, the heat loads at the source are evaluated using equations (28) through (32) by assuming an ambient temperature of 27 °C and maximum possible values for the active heat loads. The sum of the heat loads is equated with the required cooling power given by equation (11). Knowing the TEC parameters (given in Appendix A) and setting the cold temperature equal to 0.3 °C, the hot temperature,  $T_H$ , at the sink is evaluated, using equation (11), to be 30.7 °C. Substituting these temperatures into equation (17), the heating power at the sink is obtained. Since, in the worst case, this heating power is dissipated only by radiation, substituting its value in equation (33) defines the heat-sink surface area required (104.5 cm<sup>2</sup>). In reality, a considerable amount of the heating power is dissipated by conduction rather than only through radiation. Therefore, for mechanical assembly considerations, the heat sink used is only half of the calculated area given above. However, extensive testing has proven that the reduced heat sink area is sufficient under all expected operating conditions.

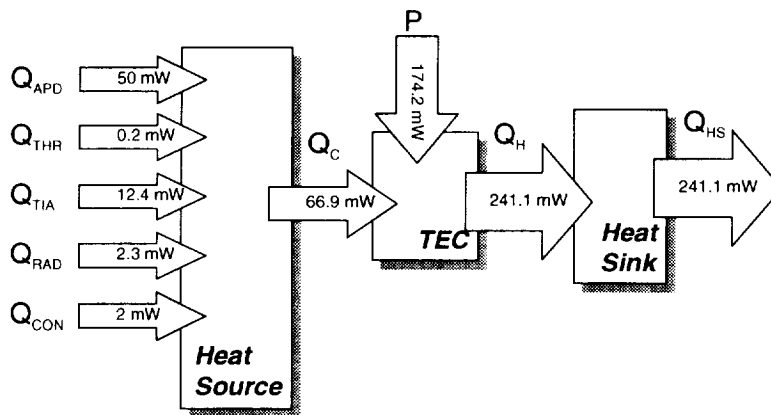


Figure 6. Power flow diagram for the APD cooling system.

## 6. Controller Performance

Referring to equation (23), the APD temperature is set to 0.3 °C by setting  $R_S$  equal to 33 k $\Omega$ . For an initial APD temperature of 23.6 °C, figure 7 shows the transient response of the APD temperature monitor voltage  $V_{TM}$ , the thermistor resistance, the APD temperature, and the TEC current. The rise time is approximately 5 s, and the 5 percent settling time is approximately 50 s with about 2 °C of overshoot. The steady-state temperature was 0.3 $\pm$ 0.3 °C. The temperature measurement is obtained by converting the temperature monitor voltage to a thermistor resistance according to equation (26), and then this is further converted into temperature according to equation (22). From figure 7(a) and (c), it is interesting to note a linear relationship between the APD temperature,  $T$ , and the temperature monitor voltage,  $V_{TM}$ , over a 30 °C operating range, which can be approximated by

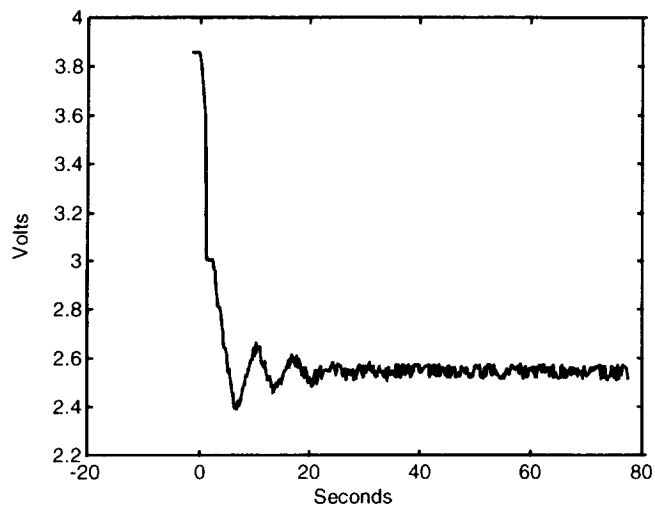
$$T \approx 17.2 \cdot V_{TM} - 43.6 \quad (34)$$

Figure 7(d) shows a steady-state TEC current of approximately 0.35 A. From equation (20), the figure of merit of the TEC is calculated to be  $1.6 \times 10^{-3}$ . From equations (16) and (18), the TEC input power is 174.2 mW, which results in a coefficient of performance equal to 38.4 percent. The maximum theoretical coefficient of performance is 39.1 percent. For successful temperature controller operation, the maximum ambient temperature is 27 °C; and since the controller was designed to cool the detector, the minimum ambient temperature is theoretically equal to the controller temperature setting.

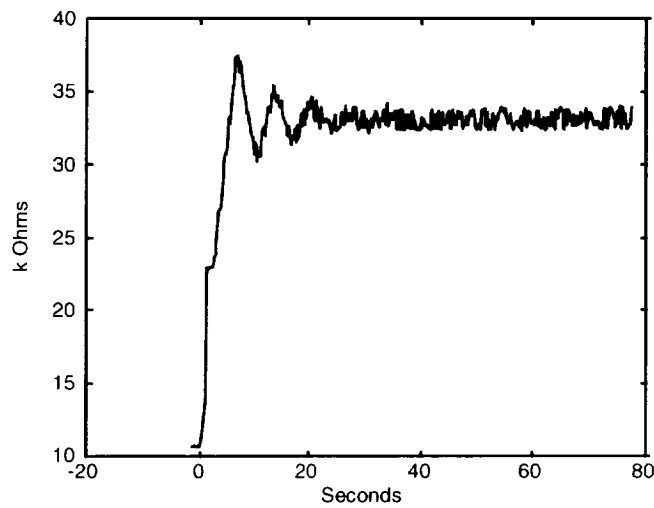
## 7. Conclusion

For this memorandum, an APD temperature controller was designed, and its performance was evaluated. The APD considered is an EG&G APD package C30649E with a built-in thermoelectric cooler, thermistor, and trans-impedance amplifier. The theory of thermoelectric cooling is discussed, and the importance of sufficient heat sinking, in order to stabilize controller operation, is shown.

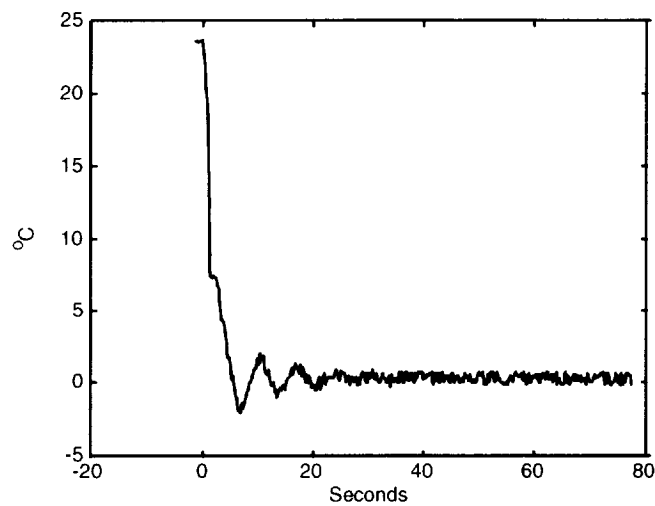
The temperature controller performance is acceptable. The final steady-state temperature of 0.3 °C and power consumption of 174.2 mW, corresponding to a 38.4 percent TEC coefficient of performance, is close to the theoretical maximum value. For successful operation, the maximum allowable ambient temperature variation is between 27 °C maximum and a minimum equal to the temperature setting. This temperature controller design has adequate accuracy and is suitable for any APD which has a built-in or external thermoelectric cooler and a temperature feedback element. The design can be simply changed to meet any temperature setting, assuming that it is below the ambient temperature. Other advantages of this controller circuit are its simplicity, low-cost, and compactness.



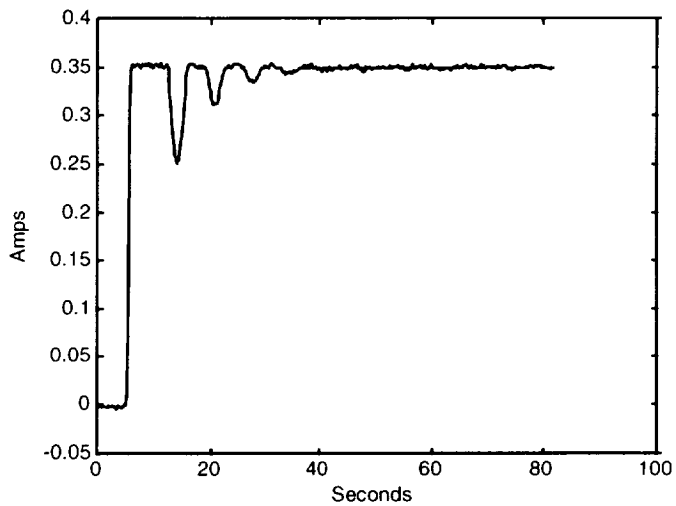
(a) Temperature Monitor Output



(b) Thermistor Variation



(c) APD Temperature Variation



(d) TEC Current

Figure 7. APD temperature and temperature monitor transients.

## References

1. B. Salah & M. Teich, *Fundamentals of Photonics*, Wiley Interscience Publication, 1991
2. T. Refaat, G. Halama & R. DeYoung, "Characterization of Advanced Avalanche Photodiodes for Lidar Receivers", *NASA/TP*, under review.
3. EG&G SLIK APD C30649E data sheet.
4. T. Refaat, W. Luck & R. DeYoung, "Design of advanced atmospheric water vapor differential absorption lidar (DIAL) detection system", *NASA/TP-1999-209348*, July 1999.
5. T. Refaat, W. Luck & R. DeYoung, "Advanced Detector and Waveform Digitizer for Water Vapor DIAL Systems", *19<sup>th</sup> International Laser Radar Conference*, Annapolis, 1998.
6. T. Refaat, W. Luck & R. DeYoung, "Advanced Water Vapor DIAL Detection System", *Conference on Lasers and Electro Optics*, 1999.
7. C. Crowell & S. Sze, "Temperature Dependence of Avalanche Multiplication in Semiconductors", *Applied Physics Letters*, Vol. 9, No 6, pp 242-244, 1966.
8. J. Conradi, "Temperature Effects in Silicon Avalanche Diodes", *Solid State Electronics*, Vol. 17, pp. 99-106, 1974.
9. R. Boyd, *Radiometry and the Detection of Optical Radiation*, Wiley, New York, 1983.
10. G. Agrawal, *Fiber-Optic Communication Systems*, Wiley, New York, 1997.
11. H. Goldsmid, *Electronic Refrigeration*, Pion Limited, 1986.
12. Marlow Industries, Inc. "Thermoelectric Cooling Systems Design Guide", Publication No 017-7939, Rev 1, 1994.
13. A. Kapitulnik, "Thermoelectric cooling at very low temperature", *Applied Physics Letters*, 60, 1992.

## Appendix A: EG&G C30649E Detector Package

### A1 Manufacturer Test Data Sheet

DESCRIPTION	CONDITION	MIN.	DATA	MAX.	UNITS
Positive Bias Current	Vr, dark, 25 °C	11	18	22	mA
Negative Bias Current	Vr, dark, 25 °C	5	7.1	15	mA
Output Offset Voltage	Vr, dark, 25 °C	-1.5	0.19	0.5	V
APD Breakdown Voltage	Ihv=2uA, dark, 25 °C	325	356	500	V
APD Operating Voltage	Resp=50 MV/W, 25 °C	300	349	480	V
APD Dark Current	Vr, dark, 25 °C	===	7	35	nA
Spectral Noise Peak	Vr, dark, 25 °C	===	150	150	nV/ $\sqrt{\text{Hz}}$
Noise Equivalent Power	Vr, dark, 25 °C	===	0.003	0.006	pW/ $\sqrt{\text{Hz}}$
APD Operating Voltage	Resp=50 MV/W, 0 °C	290	336	470	V
APD Dark Current	Vr, dark, 0 °C	===	4	15	nA
Spectral Noise Peak	Vr, dark, 0 °C	===	140	150	nV/ $\sqrt{\text{Hz}}$
Noise Equivalent Power	Vr, dark, 0 °C	===	0.003	0.006	pW/ $\sqrt{\text{Hz}}$
Bandwidth	Ihv=2uA, dark, 25 °C	10	11	===	MHz

Test are done at  $\pm 5V$  on the amplifier with  $50\Omega$  AC coupled.

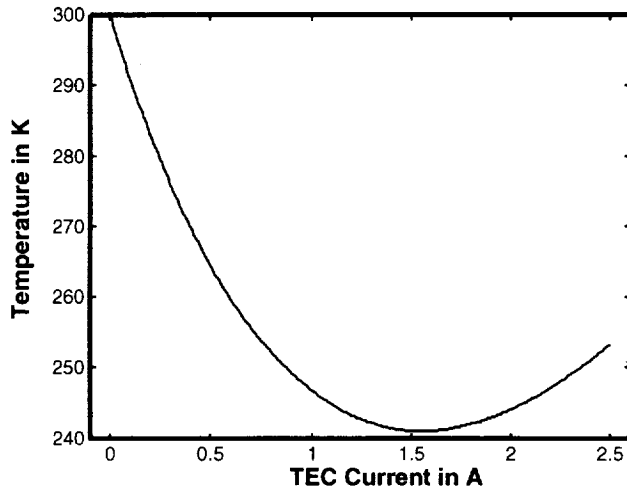
Test wavelength is 820 nm.

Serial Number 147

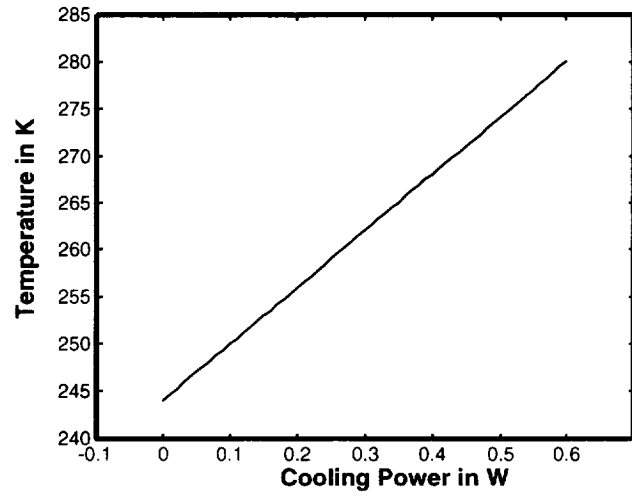
### A2 Parameters

$A_{APD}$	Detector Sensitive Area	0.24 mm <sup>2</sup> (measured)
$R_F$	Trans-Impedance Amplifier Feedback Resistance	560 k $\Omega$
$Q_{APD}$	Detector Maximum Power Loss	50 mW
$I_{max}$	TEC Maximum Current	1.8 A
$I_0$ °C	TEC Rated Current @ 0 °C	0.5 A
$A_{TEC}$	TEC Area	3.96x3.96 mm <sup>2</sup>
$R$	TEC Electrical Resistance	0.4833 $\pm$ 0.1 $\Omega$
$K$	TEC Thermal Conductance	0.0102222 W/°C
$\alpha$	Differential Seebeck Coefficient	3.2222x10 <sup>-3</sup> W/AK
$L_p$	APD Surface - Window Distance	5 mm
$R_T$	Thermistor Resistance	$R_T = 10^4 \cdot e^{\left[ \frac{3940}{T} - \frac{1}{298} \right]}$

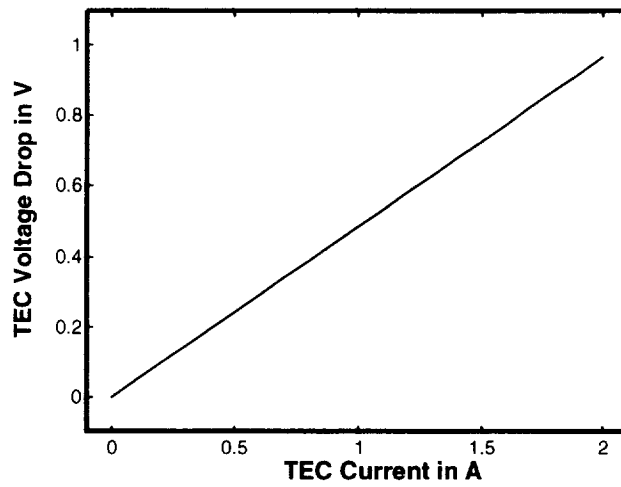
### A3 TEC Characteristics Curves



(a)



(b)

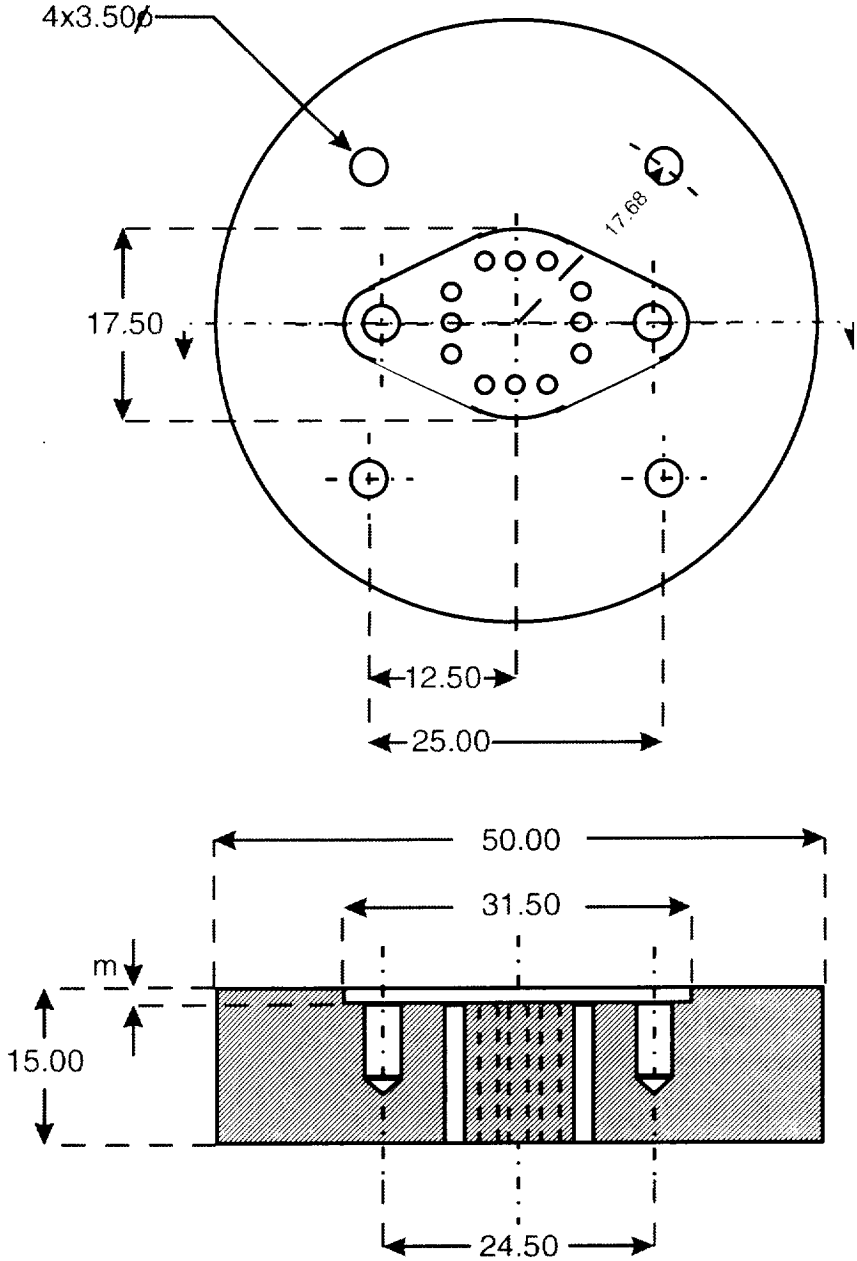


(c)

(a) Cold side Temperature,  $T_C$ , versus TEC current,  $I$ , at cooling power,  $Q_C=0$  with still air and  $T_H=300K$ . (b) Cold side Temperature,  $T_C$ , versus cooling power,  $Q_C$ , at TEC current,  $I=2A$  with still air and  $T_H=300K$ . (c) TEC current,  $I$ , versus TEC voltage drop at  $T_H=T_C=300K$ .

# Appendix B: Applied Temperature Controller System

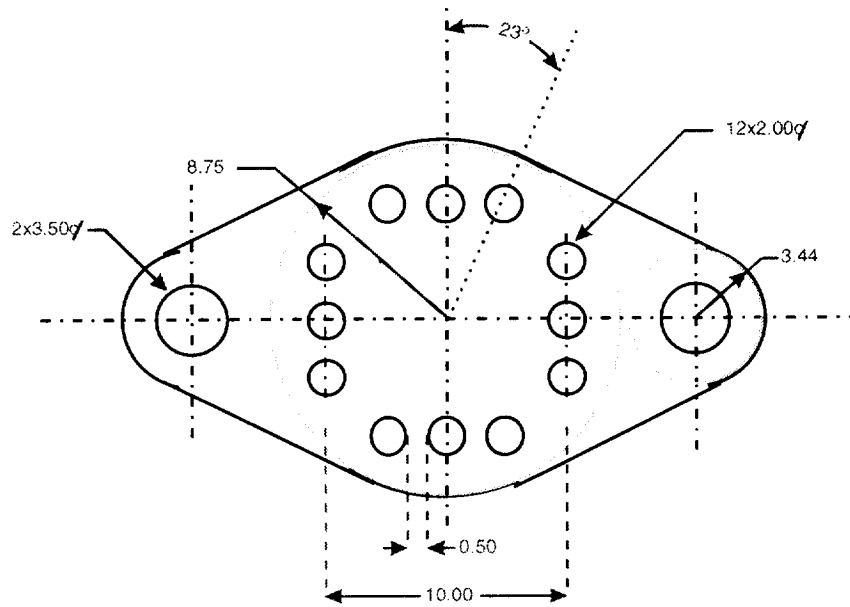
## B1 Heat Sink Design



$m = 1.5 + \text{Screw Head}$

Dimension in mm  
Material: Aluminum

## B2 Dimension of the APD Package



Dimension in mm

## B3 Temperature Controller Parameters

$V_{CC}$	Power Supply Voltage	12 V
$V_Z$	Zener Diode Voltage	5.1 V
$R_Z$	Zener Diode Current Limiting Resistor	2 k $\Omega$
$R_S$	Temperature Setting Resistance	33 k $\Omega$
$R_C$	Integration Time Constant Resistance	200 k $\Omega$
C	Integration Time Constant Capacitance	2 $\mu$ F
$R_P$	Transistor Gain Control Resistance	10 k $\Omega$
$R_L$	TEC Current Limiting Resistor	5 $\Omega$



REPORT DOCUMENTATION PAGE			Form Approved OMB No. 0704-0188	
Public reporting burden for this collection of information is estimated to average 1 hour per response, including the time for reviewing instructions, searching existing data sources, gathering and maintaining the data needed, and completing and reviewing the collection of information. Send comments regarding this burden estimate or any other aspect of this collection of information, including suggestions for reducing this burden, to Washington Headquarters Services, Directorate for Information Operations and Reports, 1215 Jefferson Davis Highway, Suite 1204, Arlington, VA 22202-4302, and to the Office of Management and Budget, Paperwork Reduction Project (0704-0188), Washington, DC 20503.				
1. AGENCY USE ONLY (Leave blank)		2. REPORT DATE October 1999	3. REPORT TYPE AND DATES COVERED Technical Memorandum	
4. TITLE AND SUBTITLE Temperature Control of Avalanche Photodiode Using Thermoelectric Cooler			5. FUNDING NUMBERS WU 622-63-13-70	
6. AUTHOR(S) Tamer F. Refaat, William S. Luck, Jr., and Russell J. DeYoung				
7. PERFORMING ORGANIZATION NAME(S) AND ADDRESS(ES) NASA Langley Research Center Hampton, VA 23681-2199			8. PERFORMING ORGANIZATION REPORT NUMBER L-17906	
9. SPONSORING/MONITORING AGENCY NAME(S) AND ADDRESS(ES) National Aeronautics and Space Administration Washington, DC 20546-0001			10. SPONSORING/MONITORING AGENCY REPORT NUMBER NASA/TM-1999-209689	
11. SUPPLEMENTARY NOTES				
12a. DISTRIBUTION/AVAILABILITY STATEMENT Unclassified-Unlimited Subject Category 33 Distribution: Nonstandard Availability: NASA CASI (301) 621-0390			12b. DISTRIBUTION CODE	
13. ABSTRACT (Maximum 200 words)  Avalanche photodiodes (APDs) are quantum optical detectors that are used for visible and near infrared optical detection applications. Although APDs are compact, rugged, and have an internal gain mechanism that is suitable for low light intensity; their responsivity, and therefore their output, is strongly dependent on the device temperature. Thermoelectric coolers (TEC) offers a suitable solution to this problem. A TEC is a solid state cooling device, which can be controlled by changing its current. TECs are compact and rugged, and they can precisely control the temperature to within 0.1 °C with more than a 150 °C temperature gradient between its surfaces. In this memorandum, a proportional integral (PI) temperature controller for APDs using a TEC is discussed. The controller is compact and can successfully cool the APD to almost 0 °C in an ambient temperature environment of up to 27 °C.				
14. SUBJECT TERMS APD; TEC; PI controllers; Temperature controllers			15. NUMBER OF PAGES 21	
			16. PRICE CODE A03	
17. SECURITY CLASSIFICATION OF REPORT Unclassified	18. SECURITY CLASSIFICATION OF THIS PAGE Unclassified	19. SECURITY CLASSIFICATION OF ABSTRACT Unclassified	20. LIMITATION OF ABSTRACT UL	



---